Available online at www.sciencedirect.com
SCIENCE DIRECT®
Acta Materialia 53 (2005) 1771–1781
Acta MATERIALIA
www.actamat-journals.com

A phase field model for the simulation of grain growth in materials containing finely dispersed incoherent second-phase particles

N. Moelans *, B. Blanpain, P. Wollants

Department of Metallurgy and Materials Engineering, Katholieke Universiteit Leuven, Kasteelpark Arenberg 44, B-3001 Leuven, Belgium

Received 5 November 2004; received in revised form 9 December 2004; accepted 10 December 2004
Available online 21 January 2005

Abstract

A phase field model is presented for simulating grain growth in materials containing small incoherent second-phase particles that are constant in time. The model of [L.-Q. Chen, W. Yang, Phys. Rev. B 50 (1994) 15752] for grain growth in single phase materials, that represents a polycrystalline microstructure with a set of phase field variables $\eta_i(\mathbf{r},t)$, has been modified to incorporate the presence of second-phase particles by adding an extra term $\epsilon\Phi\sum_i\eta_i^2$ to the free energy expression, with Φ a spatially dependent parameter that equals one inside the particles, and zero elsewhere and ϵ a positive constant. The interaction between a particle and a diffuse interphase is analyzed from an energetic point of view and the effect of pinning particles on the shape and the evolution of an initially spherical grain is studied for two-dimensional and three-dimensional systems.

Keywords: Grain growth; Zener pinning; Phase field models; Micorstructure; Simulation

1. Introduction

Small second-phase particles, such as precipitates and insoluble inclusions, exert a strong *pinning* effect, also called Zener pinning, on grain boundaries. They affect the mobility of grain boundaries and eventually arrest grain growth. The pinning effect of particles is of great practical importance in the manufacturing of high-quality materials for structural applications, where a small grain size is often required to obtain good strength and toughness.

Polycrystalline materials try to reduce their energy content by reducing the amount of grain boundary area. Due to the curvature of the grain boundary, the resultant of the surface tension [1] σ_{gb} forces the grain boundary to move towards its center of curvature, as is shown in Fig. 1. Small grains, usually having convex grain boundaries, will shrink and disappear and large grains, usually having concave grain boundaries, will grow. This results in a decrease of grain boundary area and an increase of the mean grain size. Assuming that the radius of curvature is proportional to the mean radius R of the grain, the local driving pressure P for grain growth can be formulated as [2]

$$P = \frac{\alpha\sigma_{gb}}{R} \tag{1}$$

* Corresponding author. Tel.: +32 163 212 78; fax: +32 163 219 91.
E-mail address: nele.moelans@mtm.kuleuven.ac.be (N. Moelans).

[1] In this article, no distinction is made between surface tension (N/m) and specific surface energy (J/m^2), since both are related and equal in magnitude. Specific surface energy is equal to the work performed in moving the force resulting from surface tension when the interface is increased with a unit of area.

1359-6454/$30.00
doi:10.1016/j.actamat.2004.12.026

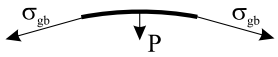

Fig. 1. σ_{gb} is the surface tension exerted on grain boundaries. Due to the curvature of the grain boundary there is a resulting driving pressure P that forces the grain boundaries to move towards their center of curvature.

with α a geometric constant which equals 2 for a spherical grain.

As a grain boundary intersects a particle, grain boundary area is reduced with an amount equal to the intersection area of particle and grain boundary. Therefore particles exert a back stress on moving grain boundaries. Zener [3] was the first to describe quantitatively the pinning effect of second-phase particles. When a grain boundary passes an immobile, incoherent particle, a force equal to

$$F_Z = 2\pi r\sigma_{gb}\cos\beta\sin\beta \tag{2}$$

with r the particle radius and the angle β as illustrated in Fig. 2, is exerted on the grain boundary. Since the surface tensions associated with the particle–matrix interface $\sigma^1_{p/m}$ and $\sigma^2_{p/m}$ cancel each other, the pinning force of a particle does not depend on them. The force is maximal when the grain boundary meets the particle at 45°:

$$F_Z^{max} = \pi r\sigma_{gb}. \tag{3}$$

This is defined as the pinning force per particle. Alternatively, the same expression for the pinning force of a particle was derived from energy considerations [4,5].

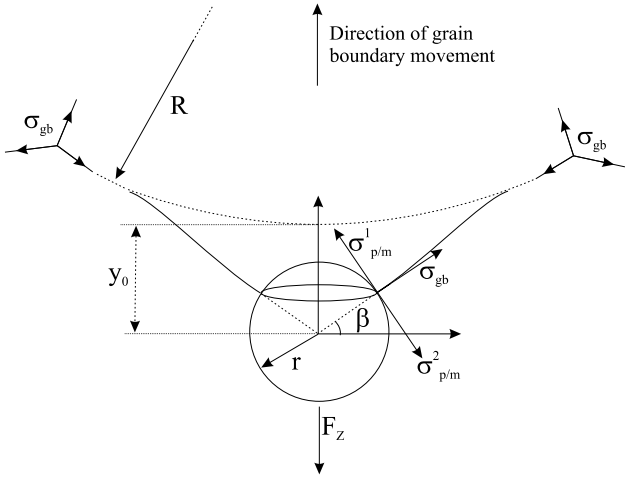

Fig. 2. Interaction between a spherical particle and a grain boundary that meets the particle at an angle β. Due to surface tensions $\sigma_{gb}, \sigma^1_{p/m}$ and $\sigma^2_{p/m}$ associated with the grain boundary and the particle–matrix interfaces, a force is exerted on the particle along the triple line where the grain boundary and the particle–matrix interface intersect, which has a length equal to $2\pi r\cos\beta$. For an incoherent and isotropic particle–matrix interface $\sigma^1_{p/m}$ and $\sigma^2_{p/m}$ cancel each other. The total force exerted on the particle equals $2\pi r\cos\beta\sigma_{gb}$ multiplied by $\sin\beta$, since all contributions perpendicular to the direction of grain boundary movement cancel. When the particle is immobile, from the action–reaction principle, the same force is exerted by the particle on the grain boundary.

When a grain boundary and a particle intersect at the meridian of the particle, the total energy of the system is reduced with an amount $\Delta F = \pi r^2\sigma_{gb}$, where πr^2 is the intersection area. To remove the particle from the boundary, a mean force equal to $\Delta F/r$ must be applied, in the direction of grain boundary movement, over a distance r, to move the grain boundary from the meridian of the particle to just beyond the particle. Both positions are shown in Fig. 3.

To calculate the pinning pressure exerted by a distribution of particles, characterized by particle radius r and volume fraction f_V of the particles, Zener assumed that grain boundaries are flat and randomly distributed with respect to the particles, that only particles located within a distance r behind a grain boundary contribute to the pinning pressure and that all contributing particles exert the maximum pinning force. Then the pinning pressure exerted by a particle distribution on a unit area of grain boundary is equal to

$$P_Z = \frac{3f_V\sigma_{gb}}{4r}. \tag{4}$$

When the pinning pressure of the particles is equal to the driving pressure for grain growth, i.e., when

$$\frac{\alpha\sigma_{gb}}{\overline{R}} = \frac{3f_V\sigma_{gb}}{4r}, \tag{5}$$

grain growth ceases. For α equal to one, the famous Zener relation

$$\overline{R}_{lim} = \frac{4r}{3f_V} \tag{6}$$

for prediction of the limiting mean grain size from the size and volume fraction of the particles, is obtained.

In reality, grain boundaries are not flat but obtain a 'dimple' or 'catenoid'-like shape near particles. Particles can therefore pin grain boundaries over a distance y_0 (indicated on Fig. 2) that is greater than r, the radius of the particles. Analytical descriptions for the shape of grain boundaries near a particle intersection were given in [6,7] and an alternative for the Zener relation that considers the dimple shape near particles,

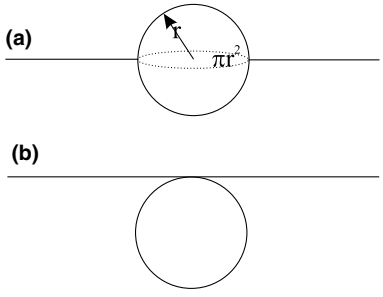

Fig. 3. Geometry used in the derivation of the pinning force of a particle from an energy principle: (a) grain boundary at the meridian of the particle, i.e., point of maximum energy reduction; (b) grain boundary just beyond the particle.

$$\overline{R}_{\mathrm{lim}} = \frac{4r}{9f_{\mathrm{V}}^{0.93}} \tag{7}$$

was proposed in [6]. Furthermore, since grain boundaries are pinned by the particles, they are not at all randomly distributed with respect to the particles. An alternative approach, that is often used for high volume fractions or strong pinning forces of the particles, consists of assuming that unpinning is extremely difficult and eventually most particles are in contact with a grain boundary. Then the relations

$$\overline{R}_{\mathrm{lim}} \propto \frac{r}{f_{\mathrm{V}}^{1/2}} \quad \text{or} \quad \overline{R}_{\mathrm{lim}} \propto \frac{r}{f_{\mathrm{V}}^{1/3}} \tag{8}$$

were derived, respectively, for two-dimensional (2D) [8] and three-dimensional (3D) systems [9]. Many more suggestions were made to improve the Zener relation [10,11], but, as the grain boundary configuration is in a complex way correlated to the particle distribution, there is no consensus yet. The shape of a grain boundary near a particle intersection depends on local parameters, such as the ratio between particle size and grain size and the surface tensions of grain boundaries and particle–matrix interfaces, but is also governed by surface tension balance requirements at the triple points where the grain boundary meets other grain boundaries (see Fig. 2). Although the assumptions Zener made are crude and the Zener relation is known to underestimate the pinning effect of a particle distribution, relation (6) is still most frequently used in practical applications for predicting the limiting mean grain radius.

Grain growth in the presence of second-phase particles has also been extensively studied from Monte Carlo simulations. The main advantage of simulation techniques is that the whole microstructure, namely the shape of the grain boundaries and the position of the particles, is calculated as a function of time. Consequently, no assumptions on the particle distribution or the shape of the grain boundaries are required. Furthermore, parameters can be varied easily and independently from each other. But simulations are very computation intensive and time consuming. Only a small number of parameter combinations could be considered up to now and the size of the systems is limited because of limitations on computer memory. The first Monte Carlo simulations for 2D systems were presented in [8] and for 3D systems in [12]. The fraction of particles located on grain boundaries ϕ was close to unity for the 2D simulations and ranged between 0.4 and 0.6 for the 3D simulations. The relation between the limiting mean grain radius $\overline{R}_{\mathrm{lim}}$ and the radius r and volume fraction f_{V} of the particles was close to relations (8). Many subsequent Monte Carlo simulations resulted in essentially the same conclusions [13–16], except those in [17,18]. According to [17], it is important to reproduce the dimples near particle intersections to obtain the correct pinning and unpinning behavior. This was not the case in the simulation experiments in [8,12], resulting in an overestimation of the pinning capacity of the particles. These findings were applied in highly large scale 3D Monte Carlo simulations [18], giving a limiting mean grain radius that is proportional to $1/f_{\mathrm{V}}$.

Still, there are materials containing pinning particles that show a grain growth behavior that does not correspond to the Monte Carlo simulations from [8,12] nor those from [17,18]. For example the austenitic Fe-0.09–0.53 mass% C-0.02 mass% P-steel containing Ce_2O_3 and CeS inclusions, studied in [19]. For this material, ϕ is between 0.1 and 0.2, which is smaller than in the Monte Carlo simulations of [8,12], although, 20–60 times greater than expected when grain boundaries are distributed randomly with respect to the position of the particles. The relation between the limiting mean grain radius and the size and volume fraction of the particles is quite different from relations obtained in the Monte Carlo simulations of [8,12] or [17,18].

Currently, the phase field method for simulating microstructure evolution is receiving much attention. Many microstructural phenomena, such as solidification, precipitation, coarsening and martensitic transformations have been simulated using the phase field method. Grain growth in single-phase materials has been simulated with the phase field method by different authors [1,20–22]. The model of [1] was extensively discussed and results were compared with experimental observations and analytical theories in [23,24]. An extension of the model towards two-phase materials was proposed by the same authors [25–27] and applied for simulating Zener pinning by growing second-phase particles in [28].

The motivation for this research was twofold. One incentive was to find out and to understand the possibilities and the limitations of the phase field method in simulating grain growth in the presence of second-phase particles. Another motivation was to perform simulations that reproduce the experimental observations from [19] and to find out which parameters are responsible for the differences in behavior between the steel containing Ce_2O_3 and CeS inclusions studied in [19] and the systems in the Monte Carlo simulations. The CeS and Ce_2O_3 particles are $\approx$200 times smaller than the austenite grains. Then the model from [28] is too computation intensive. The main purpose of the present article is therefore to introduce an alternative phase field model for simulating grain growth in materials containing incoherent second-phase particles which have a shape and size that is constant in time. It is explained how the model accounts for the presence of particles. The interaction between grain boundaries and particles in the simulated systems is studied from an energetic point of view and the shape evolution of an initially spherical grain that is pinned by particles is simulated. In a subsequent article [29], simulations for polycrystalline systems

are presented and results are compared with the experimental findings of [19] and others, analytical theories and results from Monte Carlo simulations.

2. Phase field model

According to the phase field model for grain growth in single phase materials explained in [23] the following set of phase field variables

$$\eta_1(\mathbf{r},t),\eta_2(\mathbf{r},t),\ldots,\eta_p(\mathbf{r},t)$$

is used to represent the polycrystalline microstructure of the matrix phase. The η_i distinguish the different orientations of the grains. They are continuous functions of spatial coordinates and time. Within a grain labelled by η_i, η_i equals 1 or -1, while all other phase field variables equal 0. At a grain boundary the η_i vary continuously between their equilibrium values in the neighboring grains, for example at a grain boundary between two grains labelled by $\eta_i = 1$ and $\eta_j = 1$, η_i and η_j vary between 0 and 1, while all other phase field variables are 0. Consequently grain boundaries are diffuse and have a finite thickness. Using p phase field variables, there are $2p$ possible orientations a grain can have. In real materials the number of orientations is infinite. However, for single-phase materials it was shown that p equals 36 suffices for realistic 2D grain growth simulations [23].

The total free energy of an inhomogeneous system, where properties are a function of the spatial coordinates, can be written as [30]

$$F^{\mathrm{m}} = \int_{\mathrm{V}} \left[f_0^{\mathrm{m}}(\eta_1(\mathbf{r}),\eta_2(\mathbf{r}),\ldots,\eta_p(\mathbf{r})) + \sum_{i=1}^{p} \frac{\kappa_i}{2}(\nabla\eta_i(\mathbf{r}))^2 \right] \mathrm{d}^3\mathbf{r}, \tag{9}$$

where f_0^{m} is the free energy density of the matrix phase as a function of the field variables and κ_i are the gradient energy coefficients, which are always positive so that local inhomogeneities are energetically unfavorable. Since the bulk energy of the matrix phase f_0^{m} is independent of the orientation, the free energy density functional must have $2p$ minima with equal depth, located at

$$(\eta_1,\eta_2,\ldots,\eta_p) = (1,0,\ldots,0),(0,1,\ldots,0),\ldots,(0,0,\ldots,1),(-1,0,\ldots,0),\ldots$$

reflecting the $2p$ orientations a grain can have. In [23] the following free energy density functional was assumed:

$$f_0^{\mathrm{m}}(\eta_1,\eta_2,\ldots,\eta_p) = \sum_{i=1}^{p}\left(-\frac{\alpha}{2}\eta_i^2 + \frac{\alpha}{4}\eta_i^4\right) + \gamma\sum_{i=1}^{p}\sum_{j\neq i}^{p}\eta_i^2\eta_j^2 \tag{10}$$

with α and γ positive constants and $\gamma > \alpha/2$ to have $2p$ degenerate minima. For a particular phase field variable η_i, f_0^{m} has minima at $\eta_i = \pm 1$ when all the other phase field variables equal zero, since then $\sum_{i=1}^{p}\sum_{j\neq i}^{p}\eta_i^2\eta_j^2 = 0$. If one of the other phase field variables equals 1 or -1, f_0^{m} has one minimum for η_i at $\eta_i = 0$, since the third term in the free energy density expression makes it energetically unfavorable to have two phase field variables different from zero.

When the particle–matrix interfaces are incoherent, the pinning force of a particle mainly depends on the grain boundary energy and the size of the particles. The structure and the composition of the particles are of minor importance. If it is further assumed that the shape and size of the particles is constant in time, the presence of the particles can be introduced into the model by adding the following term to the free energy density expression

$$f_0^{\mathrm{p}} = \epsilon\Phi\sum_{i=1}^{p}\eta_i^2 = \epsilon\Phi^2\sum_{i=1}^{p}\eta_i^2 \tag{11}$$

with Φ a spatially dependent parameter that equals 1 inside a particle and 0 in the matrix grains and $\epsilon \geqslant \alpha/2$.

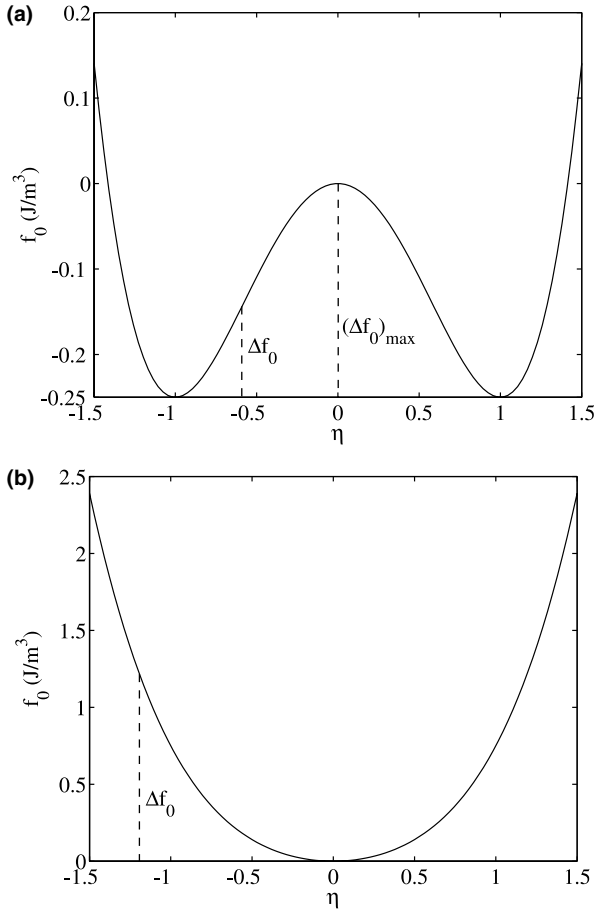

Fig. 4. Free energy density as a function of 1 order parameter and with $\alpha = \epsilon = 1$: $f_0(\eta) = -0.5*\eta^2 + 0.25*\eta^4 + \Phi\eta^2$. (a) For $\Phi = 0$: f_0 has two minima, one at $\eta = 1$ and another one at $\eta = -1$. (b) For $\Phi = 1$: f_0 has one minimum at $\eta = 0$. Δf_0 is the difference between the local free energy density and the minimum value of the free energy density for a given value of Φ.

Then the free energy density functional of the system is given by,

$$f_0(\eta_1,\eta_2,\ldots,\eta_p) = \sum_{i=1}^{p}\left(-\frac{\alpha}{2}\eta_i^2+\frac{\alpha}{4}\eta_i^4\right)+\gamma\sum_{i=1}^{p}\sum_{j\neq i}^{p}\eta_i^2\eta_j^2+\epsilon\Phi\sum_{i=1}^{p}\eta_i^2. \quad (12)$$

The extra term in the free energy forces all η_i to equal 0 inside a particle. In fact, Φ can be considered as an extra phase field variable which is constant in time. The value of Φ affects the phase field variables in the same way as the value of one of the p phase field variables affects the value of the other $p-1$ phase field variables. For $\Phi = 1$, the free energy density as a function of the η_i, $i = 1,\ldots,p$ has one minimum at all η_i equal 0. For $\Phi = 0$, the free energy density reduces to f_0^{m} with its $2p$ minima representing the different orientations of the matrix grains. The shape of the free energy density as a function of one orientation variable for $\Phi = 0$ and $\Phi = 1$ is shown in Fig. 4.

From a mathematical point of view the minimization of the total free energy F of the system, given by

$$F = \int_{\mathrm{V}}\left[f_0(\eta_1(\mathbf{r}),\eta_2(\mathbf{r}),\ldots,\eta_p(\mathbf{r}))+\sum_{i=1}^{p}\frac{\kappa_i}{2}(\nabla\eta_i(\mathbf{r}))^2\right]\mathrm{d}^3\mathbf{r} \quad (13)$$

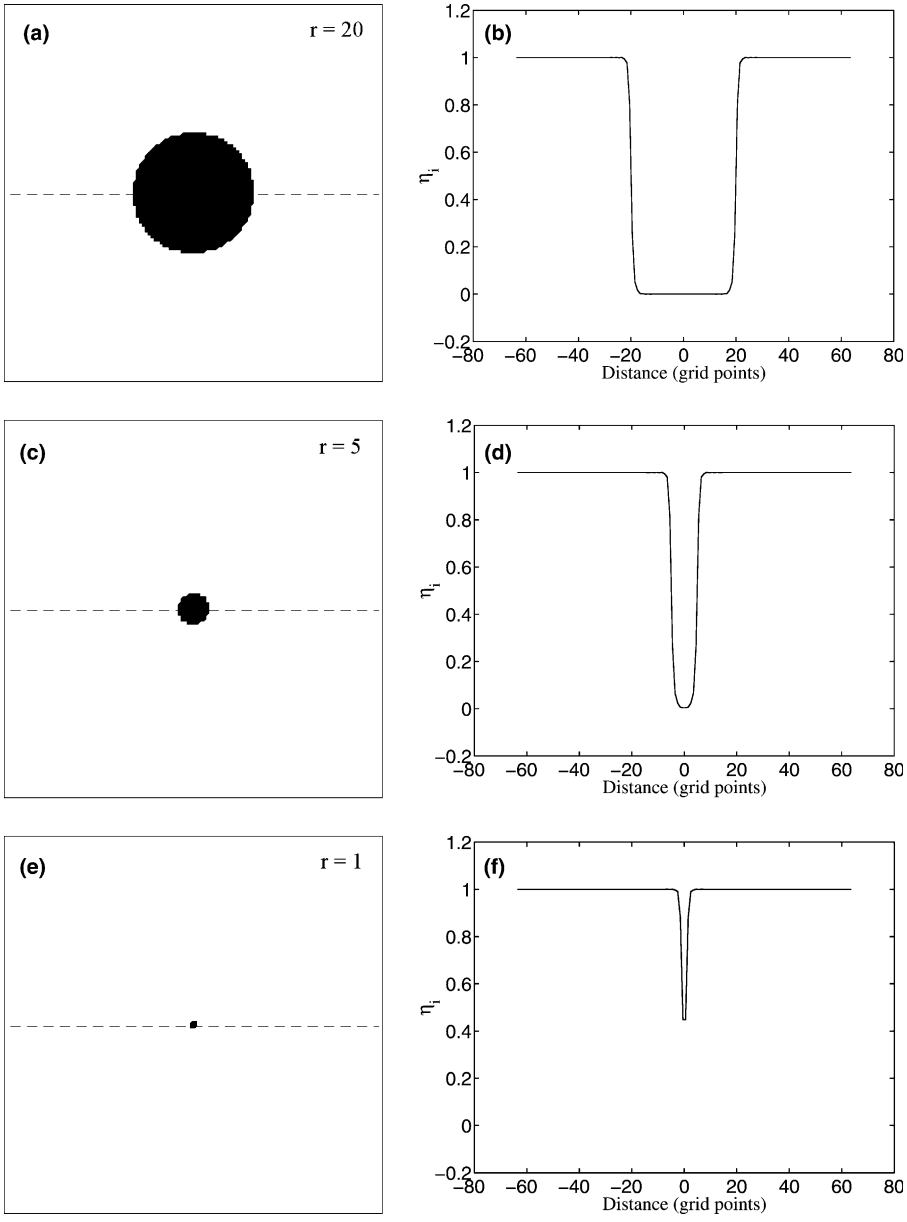

Fig. 5. Evolution of η_i across a particle located within a grain with orientation i, for particle radii equal to 20, 5 and 1 grid points and parameter values $\kappa = 0.5$, $\alpha = \gamma = \epsilon = 1$. Left: representation of Φ (2D simulation) or cross-section of Φ at the meridian of the particle (3D simulation), where black corresponds to $\Phi = 1$ and white to $\Phi = 0$. Right: evolution of η_i along the dashed line indicated in the figure on the left.

with f_0 as in (12), can be considered as the minimization of the free energy expression F^{m} (9) along with the constraint that

$$\int \frac{f_0^{\mathrm{p}}}{\epsilon}\mathrm{d}\mathbf{r} = \int \Phi \sum_{i=1}^{p} \eta_i^2 \mathrm{d}\mathbf{r} = 0. \tag{14}$$

Then ϵ is a Lagrange multiplier. Since the integrant $\Phi\sum_{i=1}^{p}\eta_i^2$ can only be positive or zero, (14) implies that $\Phi\sum_{i=1}^{p}\eta_i^2$ has to equal 0 in each point of the microstructure.

The spatial and temporal evolution of the non-conserved phase field variables is described by the time-dependent Ginzburg–Landau equation,

$$\begin{aligned}\frac{\partial \eta_i(\mathbf{r},t)}{\partial t} &= -L_i \frac{\partial F}{\partial \eta_i(\mathbf{r},t)} \\ &= -L_i\left(\frac{\partial f_0(\eta_1,\eta_2,\ldots)}{\partial \eta_i(\mathbf{r},t)} - \kappa_i \nabla^2 \eta_i(\mathbf{r},t)\right)\end{aligned} \tag{15}$$

for $i = 1,2,\ldots,p$. L_i are kinetic coefficients related to the grain boundary mobility and t is time. Substitution of expression (12) for the free energy density, gives the following set of kinetic equations:

$$\frac{\partial \eta_i}{\partial t} = -L_i\left(-\alpha\eta_i + \alpha\eta_i^3 + 2\gamma\eta_i\sum_{j\neq i}^{p}\eta_j^2 + 2\epsilon\eta_i\Phi^2 - \kappa_i\nabla^2\eta_i\right) \tag{16}$$

for $i = 1,2,\ldots,p$, that are to be solved to obtain the microstructure evolution.

The evolution of η_i across a particle located within a grain with orientation i is shown for different particle radii in Fig. 5. Outside the particle, where Φ equals 0, minimization of the free energy requires $\eta_i = 1$. Whereas, inside the particle, where Φ equals 1, minimization of the free energy requires $\eta_i = 0$. η_i is therefore forced to evolve continuously from 0 to 1 across the particle–matrix interface. When particles are only a few grid points, η_i cannot become equal to zero inside the particle. The presence of the particle still affects the evolution of the η_i, but it is ambiguous to quantify the size of the particle, since it is smaller than the thickness of the diffuse particle–matrix interface.

Alternatively, extra phase field variables that evolve in time, can be used for distinguishing the second-phase particles from the matrix phase [28]. Since small particles tend to shrink due to surface tension, at least one conservative variable, like the concentration of one of the components, must then be added to the set of phase field variables to prevent the second-phase from disappearing. The spatial and temporal evolution of conservative phase field variables is described by the Cahn–Hilliard equation which contains fourth order derivatives of the phase field variables to the spatial coordinates. This allows to simulate the evolution in time of a particle distribution, like the precipitation or coarsening of particles during grain growth. Such a model however is more complicated and requires more computation time.

3. Model parameters and simulation procedure

In the simulations α, γ and ϵ were all given the same value. Then the free energy density functional f_0 can be written as

$$\begin{aligned}&f_0(\eta_1,\eta_2,\ldots,\eta_p) \\ &\quad = m\left[\sum_{i=1}^{p}\left(-\frac{\eta_i^2}{2}+\frac{\eta_i^4}{4}\right) + \sum_{i=1}^{p}\sum_{j\neq i}^{p}\eta_i^2\eta_j^2 + \Phi\sum_{i=1}^{p}\eta_i^2\right].\end{aligned}$$

Further, the energy gradient coefficients κ_i were all given a same value κ and all relaxation coefficients L_i were chosen equal to 1, resulting in isotropic grain boundary mobility and grain boundary energy. Φ was generated in the beginning of each experiment as a 2D or 3D matrix containing zeros and ones. For representing a particle with radius r on position (x_1, y_1, z_1), grid points (x, y, z) of the matrix Φ that obey $(x-x_1)^2 + (y-y_1)^2 + (z-z_1)^2 \leqslant r^2$ were put equal to one, while the other points were put equal to zero.

The semi-implicit Fourier-spectral method explained in [31] was applied for the numerical solution of the phase field equations and the MATLAB® programming language was used for the implementation of the method [32]. The semi-implicit Fourier spectral method allows a step size Δt equal to one.

To show the microstructural evolution, the functional Ψ, defined as

$$\Psi(\vec{r}) = \sum_{i=1}^{p}\eta_i^2(\vec{r}) \tag{17}$$

was displayed using grey-levels with white representing high values and black low values. Then particles appear as black spots, grains are bright and grain boundaries gray. MATLAB was used, as well, for visualization and image processing of the obtained microstructures.

Simulations were performed on a IBM Pseries 630 with power4 processors of 1 GHz and 4 GB RAM. The maximum size for a 3D system was $200 \times 200 \times 200$ grid points. Then a simulation, using two order parameters (see Section 5), required ≈22 h for 4000 time steps.

4. Interaction between grain boundaries and particles – energetic considerations

4.1. Interfacial energies

In [30,33] the specific interfacial energy of a diffuse flat grain boundary, as shown in Fig. 6(a), is defined as the difference per unit area of interface between the free energy of the inhomogeneous system and the free energy of the system if all properties were homogeneous

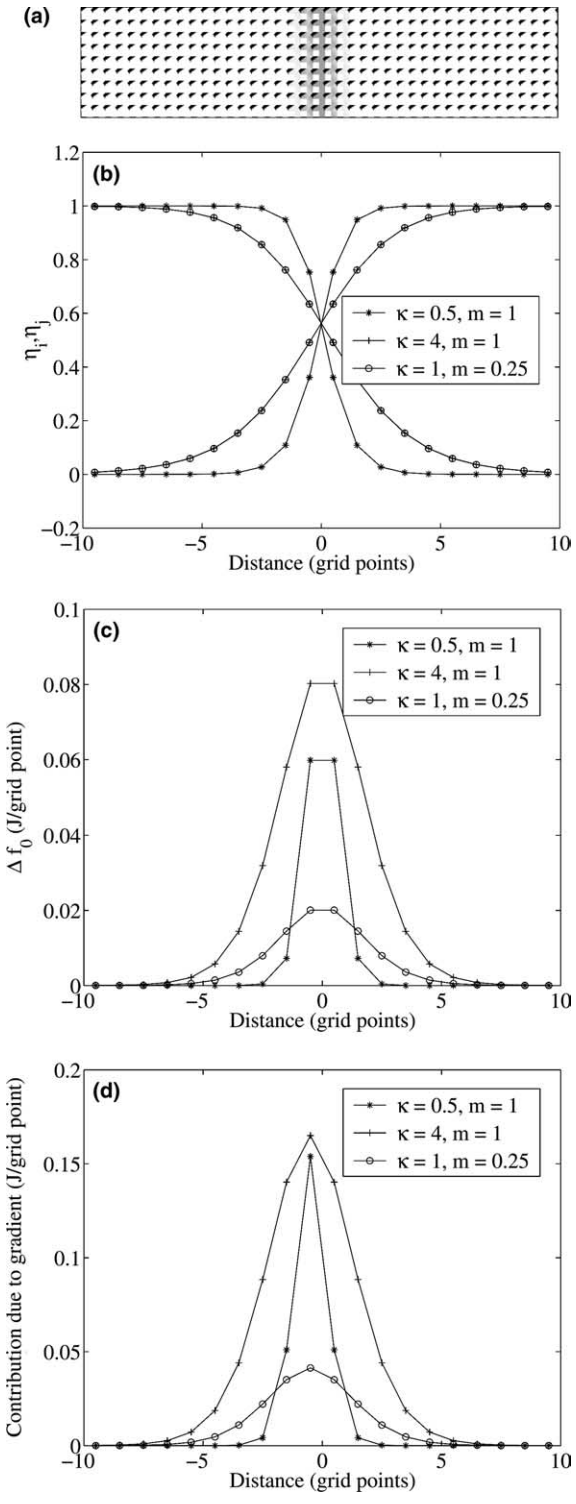

Fig. 6. (a) Flat grain boundary. (b) Evolution of η_i and η_j at a flat grain boundary between two grains with orientations i and j. (c) Evolution of Δf_0 across a flat grain boundary. (d) Evolution of $\frac{\kappa}{2}\left(\left(\frac{\partial \eta_i}{\partial x}\right)^2 + \left(\frac{\partial \eta_j}{\partial x}\right)^2\right)$ across a flat grain boundary. (c) and (d) only differ from 0 at grain boundaries.

within a grain. The specific interfacial energy of a grain boundary between two grains with orientations i and j can thus be written as

$$\sigma_{gb} = \int_{-\infty}^{+\infty} \left[f_0(0,0,\ldots,\eta_i,\eta_j,0,\ldots,0) - f_{0,\min} + \frac{\kappa_i}{2}\left(\frac{d\eta_i}{dx}\right)^2 + \frac{\kappa_j}{2}\left(\frac{d\eta_j}{dx}\right)^2 \right] dx = \int_{-\infty}^{+\infty} \left[\Delta f_0 + \frac{\kappa_i}{2}\left(\frac{d\eta_i}{dx}\right)^2 + \frac{\kappa_j}{2}\left(\frac{d\eta_j}{dx}\right)^2 \right] dx, \quad (18)$$

with $f_{0,\min} = -m/4$, the minimum of the free energy density for $\Phi = 0$, and $\Delta f_0 = f_0 - f_{0,\min}$, the difference between the local free energy density and the minimum of the free energy density, as is shown in Fig. 4. There are two contributions to the grain boundary energy. Δf_0 accounts for the fact that, across interfaces, phase field variables take values that deviate from their equilibrium values. The term with the energy gradient coefficients $\kappa_{i,j}$ accounts for the fact that properties are not homogeneous at interfaces. For a flat interface that is locally in equilibrium [30,33]

$$\Delta f_0 = \frac{\kappa}{2}\left(\frac{\partial \eta_i}{\partial x}\right)^2 = \frac{\kappa}{2}\left(\frac{\partial \eta_j}{\partial x}\right)^2 \quad (19)$$

and alternative formulations for the grain boundary energy are

$$\sigma_{gb} = 3\int_{-\infty}^{+\infty} \Delta f\, dx = \frac{3}{\sqrt{2}}\int_0^1 \sqrt{\kappa \Delta f}\, d\eta_i. \quad (20)$$

Hence, grain boundary energy is proportional to $\sqrt{\kappa}$.

The thickness l of a flat grain boundary that is locally in equilibrium is approximately proportional to [30,33]

$$l \propto \sqrt{\frac{\kappa}{(\Delta f_0)_{\max}}} \propto \sqrt{\frac{\kappa}{m}} \quad (21)$$

with $(\Delta f_0)_{\max}$ as illustrated in Fig. 4 and m as defined in Section 3. It was pointed out in [23] that, for 2D systems κ/m should be at least 4, to resolve the evolution of the phase field variables at grain boundaries, so that grain boundary mobility and grain boundary energy are reproduced properly. However, as a compromise between efficiency and accuracy, κ/m is often taken smaller than 4.

In Fig. 6(b) the evolution of η_i and η_j across a flat grain boundary between two grains with orientations i and j is shown for different values of the parameters κ and m. The combinations $\kappa = 4$ (expressed in J/grid point), $m = 1$ (expressed in J/grid point) and $\kappa = 1$, $m = 0.25$ correspond to $\kappa/m = 4$. The combination $\kappa = 0.5$, $m = 1$ was used in [23,24] in phase field simulations for normal grain growth in single-phase materials. In the Figs. 6(c) and 6(d), the behavior of both terms in the grain boundary energy are shown for the different parameter values used in Fig. 6(b). The specific grain boundary energy σ_{gb} can be calculated by numerical integration of (18). It is equal to 0.40 (ex-

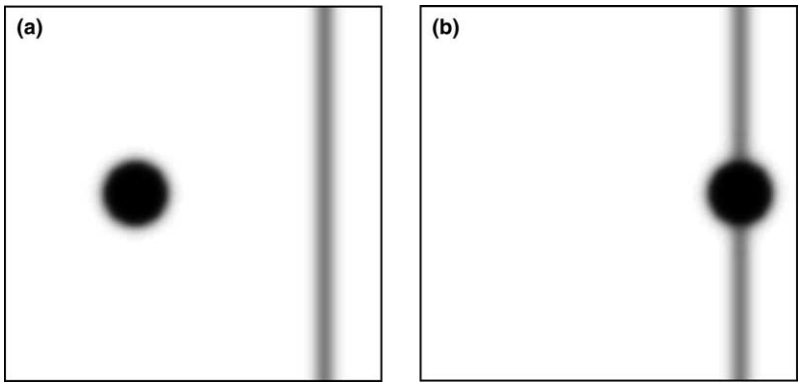

Fig. 7. Geometry used for calculating the interaction energy between particles and grain boundaries. The pinning energy is calculated as the difference between the free energy of the system on the right and the free energy of the system on the left. Illustrated for $r = 10$, $\kappa = 0.5$ and $m = 1$.

pressed in J/grid point) for $\kappa = 0.5$, $m = 1$, to 1.16 for and $\kappa = 4$, $m = 1$ and to 0.29 for $\kappa = 1$, $m = 0.25$. Numerical integration of

$$\sigma_{\mathrm{gb}} = \frac{1}{4\pi r^2}\int_{-\infty}^{+\infty}\int_{-\infty}^{+\infty}\int_{-\infty}^{+\infty}\Delta f_0 + \frac{\kappa_i}{2}\left(\left(\frac{\partial \eta_i}{\partial x}\right)^2+\left(\frac{\partial \eta_i}{\partial y}\right)^2+\left(\frac{\partial \eta_i}{\partial 7}\right)^2\right) \quad (22)$$

$$+\frac{\kappa_j}{2}\left(\left(\frac{\partial \eta_j}{\partial x}\right)^2+\left(\frac{\partial \eta_j}{\partial y}\right)^2+\left(\frac{\partial \eta_j}{\partial z}\right)^2\right)\mathrm{d}x\,\mathrm{d}y\,\mathrm{d}z \quad (23)$$

for a spherical grain that is much larger than the grain boundary thickness, gives similar results.

In analogy with expression (18), the interfacial energy of a flat particle–matrix interface for a particle located within a grain with orientation i can be written as

$$\sigma_{p/m} = \int_{-\infty}^{+\infty}\left[f_0(0,0,\ldots,\eta_i,0,\ldots,0) - f_{0,\min} + \frac{\kappa_i}{2}\left(\frac{\mathrm{d}\eta_i}{\mathrm{d}x}\right)^2\right]\mathrm{d}x. \quad (24)$$

$f_{0,\min}$ equals $-m/4$ at the matrix side of the interface and 0 at the particle side (see Fig. 4). Numerical integration gives 0.255 for $\kappa = 0.5$, $m = 1$, 0.812 for $\kappa = 4$, $m = 1$ and 0.203 for $\kappa = 1$, $m = 0.25$. Given the values for α, γ and κ, which are linked to the bulk and interfacial properties of the matrix phase, the interfacial energy of the particle–matrix interface can be adjusted by changing the value of ϵ, although the flexibility is small. ϵ must be greater than $\alpha/2$ to have the minimum of the free energy density functional at $(\eta_1, \eta_2, \ldots, \eta_p) = (0, 0, \ldots, 0)$. On the other hand, since Δf_0 increases with increasing value for ϵ and the grain boundary thickness is inversely proportional to the square root of Δf_0 (Eq. (21)), the numerical solution becomes inaccurate and even unstable for ϵ to large. For $\kappa = 0.5$, $m = 1$, the numerical solution becomes unstable at $\epsilon > 2.5$, for $\kappa = 4$, $m = 1$, at $\epsilon > 2.5$, as well and for $\kappa = 1$, $m = 0.25$, at $\epsilon > 8$. Therefore, and also because it is not one of the essential parameters, the interfacial energy of the particle–matrix interface will not be considered further in this article. If the properties of the second-phase or the particle–matrix

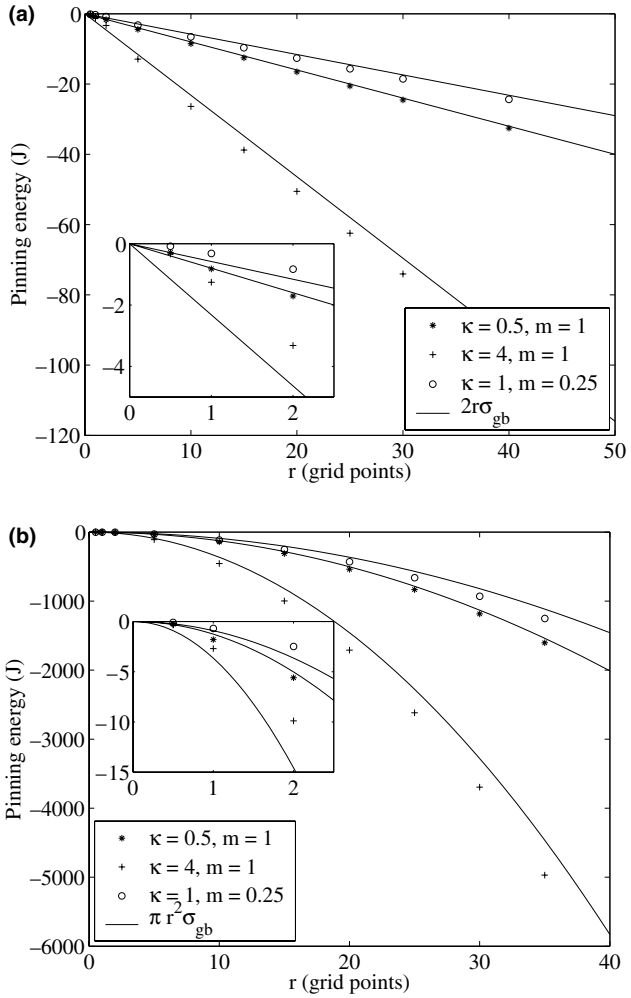

Fig. 8. Pinning energy as a function of the particle radius r, calculated by taking the difference between the free energy of the systems displayed on the right and left sides in Fig. 7 and from $2r\sigma_{\mathrm{gb}}$ for 2D simulations (a) or $\pi r^2\sigma_{\mathrm{gb}}$ for 3D simulations (b), where σ_{gb} is the specific grain boundary energy.

interface are important, another model, for example the one from [28], should be used.

4.2. Interaction energy

The interaction energy associated with a particle-grain boundary intersection can be calculated for the simulated systems by taking the difference between the free energy of a system containing a flat grain boundary and a particle that intersect, illustrated in Fig. 7 on the right, and the free energy of the system when the particle is located far from the grain boundary, illustrated in Fig. 7 on the left. As discussed in the introduction, the interaction between particles and grain boundaries is based on the fact that when a particle and a grain boundary intersect, the amount of grain boundary is reduced by the intersection length (2D) or area (3D). Accordingly, assuming the maximum intersection length $2r$ or section πr^2, the interaction energy for the simulated systems should be close to $-2\sigma_{gb}r$ or $-\pi r^2\sigma_{gb}$. In Fig. 8, the interaction energy is given for the three combinations of κ and m used before, and for different particle radii. Because of the finite thickness of the diffuse grain boundaries, also a small amount of the particle–matrix interface is removed, when a particle and a grain bound-

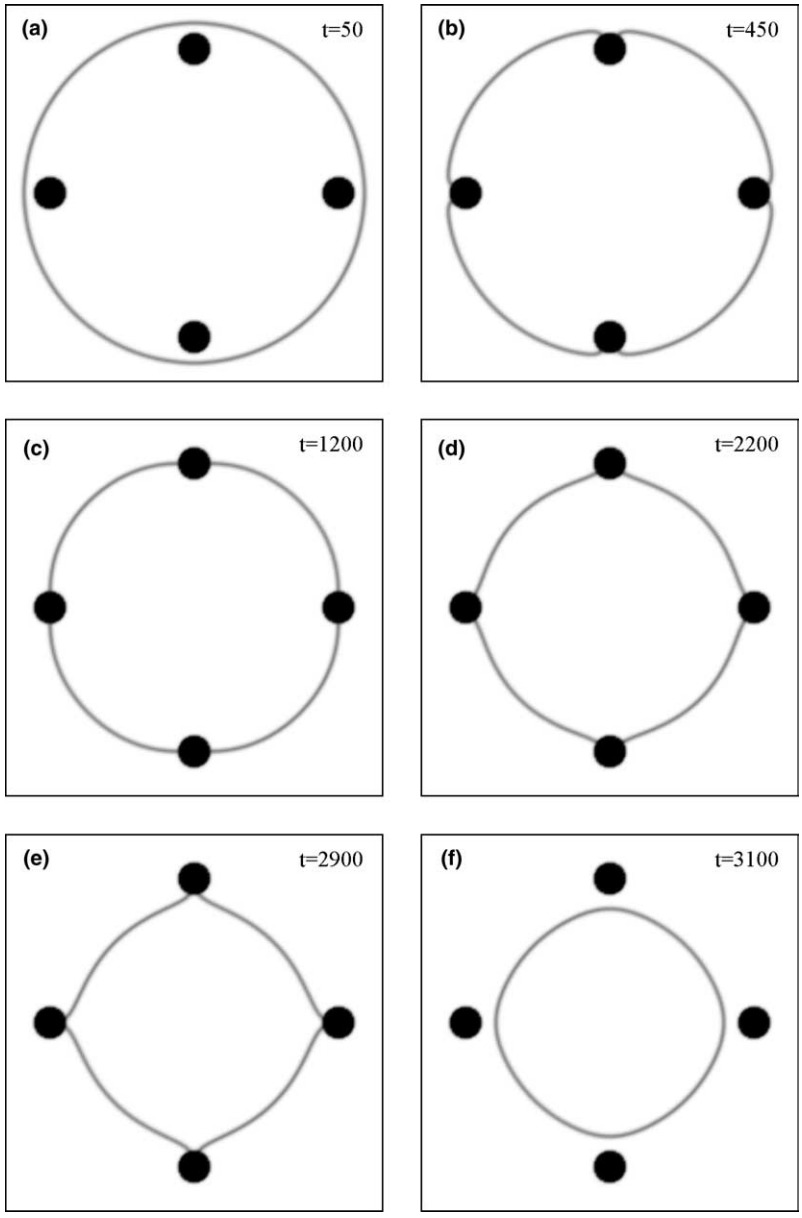

Fig. 9. Evolution of a spherical grain containing six second-phase particles, equally spaced on an inner sphere: cross-sections at the meridian of the grain for $t = 50$, $t = 450$, $t = 1200$, $t = 2200$, $t = 2900$ and $t = 3100$. Initial grain radius: $R_0 = 90$, particle radius: $r = 8$, radius inner sphere: $d = 76$, system size: $200 \times 200 \times 200$ (all expressed in grid points).

ary intersect. As a consequence, the value calculated by taking the difference in free energy between both configurations displayed in Fig. 7 is slightly more negative than the values calculated from $-2\sigma_{gb}r$ or $-\pi r^2\sigma_{gb}$. The deviation is largest for $\kappa = 4$, $m = 1$, since then the interfacial energy associated with the particle–matrix interface is the highest. Particles of a few grid points are completely surrounded by the diffuse grain boundary region, when located on a grain boundary. Then the interaction between grain boundaries and particles in the simulated systems is rather based on a reduction in particle–matrix interface instead of a reduction in grain boundary and the interaction energies deviate from the one expected from $-2\sigma_{gb}r$ or $-\pi r^2\sigma_{gb}$. For $\kappa = 0.5$, $m = 1$, giving $\kappa/m = 0.5$, this is for particle radii smaller than 2, whereas for the other two combinations with $\kappa/m = 4$, this is already for particle radii smaller than 5. The interaction energy is still negative. Therefore, particles of a few grid points pin grain boundaries as well.

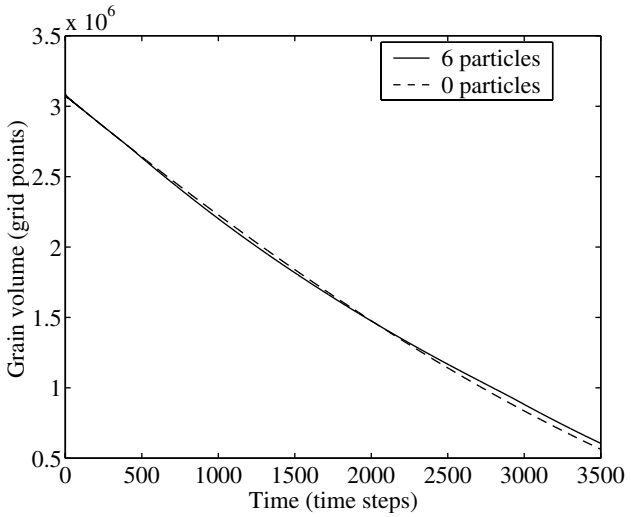

Fig. 10. Time evolution of the volume of the spherical grain containing six second-phase particles considered in Fig. 9, compared with the time evolution of the volume of a spherical grain with the same initial grain radius when no particles are present.

5. Evolution of a spherical grain in the presence of particles

Fig. 9 illustrates the temporal evolution of an initially spherical grain containing six particles equally spaced on an inner sphere. Cross-sections of the spherical grain at different time steps are shown. In Fig. 10, the evolution of the volume of the spherical grain containing six particles is compared to the evolution of the volume of a spherical grain with the same initial grain radius when no particles are present. Since grain boundaries move towards their center of curvature, the spherical grain is expected to shrink. In the beginning, when the grain boundary is far from the particles, the evolution of the grain is the same as when no particles are present. As the grain boundary approaches the particles, the boundary is locally attracted by the particles and the volume decreases faster then when no particles are present. Once the grain boundary intersects the particles, the particles locally prevent the grain boundary from further movement and the decrease in volume slows down. Because of the local character of the grain boundary–particle interactions, the spherical shape is lost. In between the particles, the grain boundary continues travelling towards the center and the angle β at which the grain boundary meets the particles increases. Although the interfaces are too thick to resolve their shape accurately, the grain boundary shows a dimple-like shape before it escapes from the particles (see the image on time step 2900 in Fig. 9). Finally, when β is beyond $\pi/4$, the grain boundary escapes from the particles. The distance over which the particles pin the grain boundary (y_0 in Fig. 2) is larger than r the radius of the particle. After escape, the grain recovers its spherical shape. The overall result is that the grain boundary mobility is lowered by the particles.

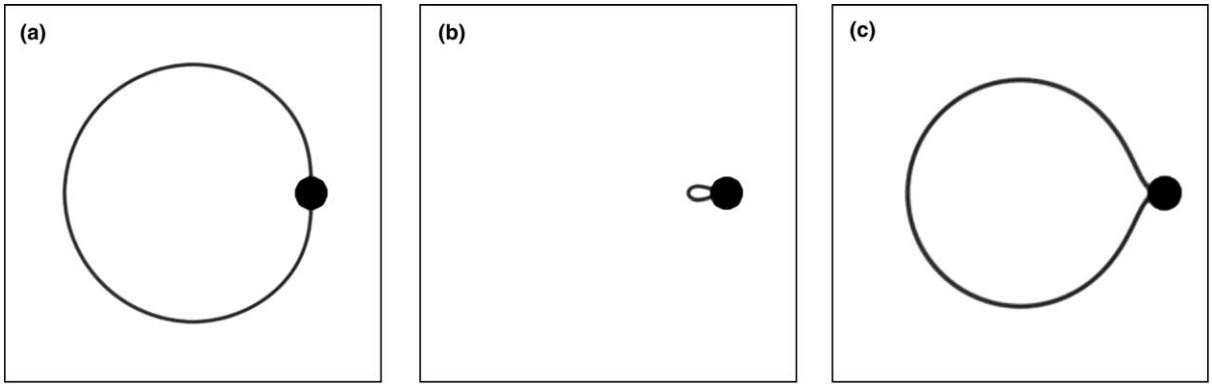

Fig. 11. The evolution of a circular grain pinned by a particle in a 2D simulation compared with the evolution of a cross-section of a spherical grain pinned by a particle in a 3D simulation. (a) Initial configuration. (b) Image just before the disappearance of the circular grain in the 2D simulation. The grain boundary could not escape from the particle. (c) Image just before the escape of the grain boundary from the particle in the 3D simulation.

For a 2D system the force exerted by a particle on a bypassing grain boundary that meets the particle at an angle β (see Fig. 2) can be derived in the same way as Zener did for 3D systems [34]:

$$F_Z^{2D} = 2\sigma_{gb} \sin \beta. \quad (25)$$

The force F_Z^{2D} is maximal for $\beta = \pi/2$ and not for $\beta = \pi/4$ as is the case in three dimensions. Therefore, the shape of a grain boundary when passing a particle in 2D systems deviates from the shape observed in cross-sections of 3D systems giving pinning and unpinning behavior that is essentially different. Since in 2D systems the maximum pinning force is only reached at $\beta = \pi/2$, it is extremely difficult for a grain boundary to escape from a particle. As shown in Fig. 11, a circular grain pinned by a single particle is not able to escape from the particle, whereas a 3D spherical grain, escapes from the particle for β slightly higher than $\pi/4$.

6. Conclusions

Although, controlling the grain size by means of second-phase particles is of high technological importance, up to now there is no consensus on the relation between the limiting mean grain size and the size and volume fraction of the second-phase particles. Often theory or simulation models are not able to explain experimental results. A phase field model for simulating grain growth in materials containing finely dispersed second-phase particles, which have a shape and size that is constant in time, is presented. The use of a spatially dependent parameter in the free energy expression for representing the particles instead of extra phase field variables, reduces the computational work considerably, although simulations are still highly computation intensive. Due to the diffuse interfaces, characteristic for phase field simulations, small particles of a few grid points are not completely resolved and for particle sizes larger than the grain boundary thickness the pinning energy is slightly too high. In 3D systems, a grain boundary escapes from a particle just beyond the point of maximum restraining force, i.e., just beyond $\beta = \pi/4$, while in 2D systems it is very difficult for a grain boundary to escape from a particle since the maximum pinning force is only reached at $\beta = \pi/2$.

Acknowledgment

This research was funded by the Institute for the Promotion of Innovation through Science and Technology in Flanders (IWT-Vlaanderen).

References

[1] Chen L-Q, Yang W. Phys Rev B 1994;50:15752.
[2] Burke J, Turnbull D. Prog Met Phys 1952;3:220.
[3] Smith C. Trans Metall Soc AIME 1948;175:15.
[4] Ashby M, Harper J, Lewis J. Trans Metall Soc AIME 1969;245:413.
[5] Ashby N. Recrystallization and grain growth of multi-phase and particle containing materials. In: Hansen N, Jones AR, Leffers T, editors. 1st Riso international symposium on metallurgy and materials science, Riso; 1980. p. 325.
[6] Hellman P, Hillert M. Scand J Met 1975;4:211.
[7] Gladman T. Proc R Soc Lond 1966;A294:298.
[8] Srolovitz D, Anderson M, Grest G, Sahni P. Acta Metall 1984;32:1429.
[9] Hillert M. Acta Metall 1988;36:3177.
[10] Humphreys F, Hatherly M. Recrystallization and related annealing phenomena. Oxford: Pergamon; 1996.
[11] Nes E, Ryum N, Hunderi O. Acta Metall 1985;33:11.
[12] Anderson M, Grest G, Doherty R, Li K, Srolovitz D. Scrip Metall 1989;23:753.
[13] Hassold G, Holm E, Srolovitz D. Scrip Metall Mater 1990;24:101.
[14] Ohnuma I, Ohtani H, Ishida K, Nishizawa T. Mater Sci For 1996;204:313.
[15] Kad B, Hazzledine P. Mater Sci Eng 1997;A238:70.
[16] Soucail M, Messina R, Cosnuau A, Kubin L. Mater Sci Eng 1999;A271:1.
[17] Miodownik M, Martin J, Cerezo A. Phil Mag A 1999;79:203.
[18] Miodownik M, Holm E, Hassold G. Scrip Mater 2000;42:1173.
[19] Guo M, Suito H. ISIJ Int 1999;39:1289.
[20] Lusk M. Proc R Soc Lond 1999;A455:677.
[21] Kobayashi R, Warren J, Carter W. Physica D 1998;119:415.
[22] Steinbach I, Pezzolla F, Nestler B, BeeBelber M, Prieler R, Schmitz G, et al. Physica D 1996;94:135.
[23] Fan D, Chen L-Q. Acta Mater 1997;45:611.
[24] Fan D, Geng C, Chen L-Q. Acta Mater 1997;45:1115.
[25] Chen L-Q, Fan D. J Am Ceram Soc 1996;79:1163.
[26] Fan D, Chen L-Q. Acta Mater 1997;45:3297.
[27] Fan D, Chen S, Chen L-Q, Voorhees P. Acta Mater 2002;50:1895.
[28] Fan D, Chen L-Q, Chen S-PP. J Am Ceram Soc 1998;81:526.
[29] Moelans N, Blanpain B, Wollants P. Acta Mater [in preparation].
[30] Cahn J, Hilliard J. J Chem Phys 1958;28:258.
[31] Chen L, Shen J. Comput Phys Commun 1998;108:147.
[32] Trefethen L. Spectral methods in MATLAB. Philadelphia, PA: SIAM, Society for Industrial and Applied Mathematics; 2000.
[33] Allen S, Cahn J. Acta Metall 1979;27:1085.
[34] Doherty R, Srolovitz D, Rollett A, Anderson M. Scrip Metall 1987;21:675.